Journal of Chromatography, 556 (1991) 457–484
Elsevier Science Publishers B.V., Amsterdam

CHROM. 23 099

Influence of solute size and the non-polar interaction term on the selection of test solutes for the classification of stationary phase selectivity in gas chromatography

THEOPHILUS O. KOLLIE and COLIN F. POOLE*
Department of Chemistry, Wayne State University, Detroit, MI 48202 (USA)

ABSTRACT

A new parameter ΔG_S^{INT} (X) is introduced for the determination of the capacity of a stationary phase to enter into orientation and hydrogen-bonding interactions. ΔG_S^{INT} (X) is defined as the component of the free energy of solution that is equivalent to the solute–solvent interactions of solute (X) that exceeds those interactions typified by an *n*-alkane of identical volume in solvent S reduced by the identical interactions of solute (X) in a hydrocarbon solvent (squalane). ΔG_S^{INT} (X) provides a quantitative scale of orientation and proton donor–acceptor interactions that is independent of solute size and non-polar solute–solvent interactions. Multivariate analysis of ΔG_S^{INT} (X) values for 21 test solutes on 20 stationary phases was used to identify acceptable test solutes for characterizing specific intermolecular interactions and to classify the stationary phases based on their capacity for these interactions. Several highly correlated solutes were identified as suitable for determining orientation and solvent proton acceptor capacity of which nitrobenzene and *n*-octanol, respectively, are recommended as the preferred solutes. Benzene and dioxane were identified as the most favorable test solutes for solvent proton donor capacity within the data set. It seems likely that a more appropriate solute could be found for this interaction. The classification of stationary phases by ΔG_S^{INT} (X) is informative and shows a logical clustering of phases of similar type and a linearly related change in properties for the homologous series of poly(methylphenylsiloxane) solvents as the mole percentage of phenyl groups is increased.

INTRODUCTION

The properties of a stationary phase that are considered important in the selection process for a particular application are its useful temperature operating range, ability to provide columns of acceptable efficiency and its characteristics as a solvent determined by its solvent strength and selectivity. The first two parameters can be determined unambiguously for any phase and limiting boundary conditions established [1]. The strength of a solvent (synonymous with the general concept of polarity) is a measure of the capacity of a stationary phase to enter into all intermolecular interactions. No exact method has emerged for calculating or determining this term, however, and its current usage is based on common sense [2,3]. It is not important to the studies reported here and will not be discussed further. The solvent selectivity is a measure of the capacity of a stationary phase to enter into specific intermolecular

0021-9673/91/$03.50

interactions represented by dispersion, induction, orientation and donor–acceptor complexation (*e.g.*, hydrogen bonding). Molecular mechanics has not reached a state of maturity, to date, that would permit the *a priori* calculation of the above forces in the complex systems represented by solute–stationary phase interactions of interest in gas chromatography. In the absence of an exact method of calculation chromatographers have come to rely upon a number of empirical experimental approaches to characterize these forces [1–6]. Of these approaches, the system of stationary phase selectivity constants introduced by Rohrschneider and later extended by McReynolds has been the most widely used and virtually all popular stationary phases have been characterized by this method. Certain theoretical and experimental deficiencies in the McReynolds approach have been recognized recently (and also in other methods based on retention index differences) and can be briefly summarized as follows [2,3,7–10]: poor retention of test solutes on some phases prevents the accurate determination of retention index values; the calculation method ignores the importance of interfacial adsorption as a retention mechanism (interfacial adsorption is often the dominant retention mechanism for *n*-alkanes on polar phases); individual phase constants are composite values defined by the retention characteristics of both the retention index standards and test solutes (the retention characteristics of the *n*-alkanes dominate in many instances); and the original data of McReynolds contains experimental uncertainties that affect their reliability. It has been suggested that the McReynolds approach to stationary phase characterization should be abandoned in favor of thermodynamic approaches which can be related to rigorous models describing the transfer of a solute from the gas phase to the stationary phase. Early thermodynamic approaches to the measurement of selectivity were based on the determination of the partial molar Gibbs free energy of solution for either functional groups [11] or specific test solutes, such as the first five test solutes suggested by McReynolds [12,13]. The sum of the retention index increments for the first five McReynolds' test solutes, suggested as a general scale of solvent polarity, was shown to correlate with the partial molar excess, Gibbs free energy of solution of a methylene group [14,15]. In more recent studies the molal standard state was adopted to minimize inconsistencies from a lack of an exact knowledge of the molecular weight of common polymeric phases [3,8,16] and multivariate analysis techniques were used to identify suitable test solutes to characterize stationary phase interactions [8,17]. For highly cohesive phases such as OV-275, TCEP and DEGS, the selectivity parameters were found to be solute-size dependent [17]. It was speculated that the size dependence for the test solutes could be removed by separating the free energy into a cavity term and an interaction term, the latter being independent of solute size and representative of polar solute–solvent interactions. The elaboration of this interaction term into a quantitative scale of solvent selectivity and the selection of test solutes to characterize specific molecular interactions are the focus of this paper.

To accommodate differences in solute size in the selectivity scale it will be necessary to employ a model which specifically incorporates a size-dependent term in the decomposition of the free energy of solution for the test solutes. Linear solvation energy relationships employing solvatochromic parameters have been very successfully applied to the prediction of a wide range of solvent properties [18–20]. In this model the solvation process is considered to involve three steps: (1) the creation of a cavity in the solvent of a suitable size to accommodate the solute; (2) reorganization

of the solvent molecules around the cavity (the free-energy change for this process is probably small or zero); and (3) interaction of a solute molecule with the surrounding solvent molecules. For transfer from the gas phase to the stationary phase the overall free energy change must be negative, the cavity formation process is endoergic (positive free-energy change) and the solute–solvent interaction term is exoergic (negative free-energy change). The solvation process is described by the general equation

$$SP = SP_o + mV_2/100 + S(\pi_2^* + d\delta_2) + a\alpha_2 + b\beta_2 \quad (1)$$

where SP is some solvent property to be correlated and SP_o is a constant. V_2 is a volume term characteristic of the solute (*e.g.*, molar volume, Van der Waals volume). The term mV_2 describes the endoergic process of cavity formation. The three solute terms π_2^*, α_2 and β_2 are the monomer solute dipolarity, hydrogen-bond acidity and hydrogen-bond basicity, respectively, and are used to characterize the exoergic solute–solvent interactions. The term containing δ_2 is a solute polarizability correction factor. There is no explicit term in eqn. 1 that corresponds to a dispersion interaction. This does not seem to matter for processes that involve condensed phases, *e.g.*, liquid–liquid distribution, because the dispersion interactions in each phase will largely cancel. However, this term cannot be neglected for the process of transferring a solute from the gas phase to solution. For such processes, the alternative eqn. 2 is preferred, with the solute parameter log K_L^{16} replacing the solute parameter $V_2/100$ [21–23]:

$$SP = SP_o + l(\log K_L^{16}) + s\pi_2^* + a\alpha_2 + b\beta_2 \quad (2)$$

Log K_L^{16} is the logarithm of the solute gas–liquid partition coefficient for hexadecane as solvent at 298 K. The function $l(\log K_L^{16})$ is related to the endoergic work of creating a cavity in the solvent and the endoergic solute–solvent dispersion interactions. Abraham *et al.* [24] have used a modified version of eqn. 2 to characterize the solvent properties of the 77 stationary phase data set of McReynolds:

$$\log V_g^0 = C + rR_2 + s\pi_2^* + a\alpha_2 + b\beta_2 + l \log K_L^{16} \quad (3)$$

where V_g^0 is the specific retention volume for the solute and R_2 is a term describing the solute molar refraction. The coefficients r,s,a,b and l, obtained by multiple linear regression, determine quantitatively the susceptibility of a stationary phase to enter into specific interactions and can be used to characterize stationary phase properties. The r coefficient determines the tendency of the phase to interact with π- or n-solute electron pairs, s phase dipolarity, a phase hydrogen-bond basicity, b phase hydrogen-bond acidity and l a combination of general dispersion interactions and cavity effects. In order to separate out effects due to cavity formation and to allow, at least partly, for solute–solvent dispersion interactions, several workers have referenced solvation properties, such as partition coefficients, to those of a non-polar solute (usually an n-alkane) with a similar volume to the solute in question [25–30]. This was the basis of the Snyder selectivity triangle approach for classifying solvents in terms of the relative strength of their orientation and hydrogen bonding interactions using nitromethane, ethanol and dioxane as test solutes [25,26,30]. In Snyder's treatment, the contribution of induction and entropy effects, etc., to the solute gas–liquid partition coefficient

were removed by subtracting the partition coefficient for a particular test solute in a hydrocarbon solvent (in fact, the average value for hexane, isooctane and cyclohexane) from the value of the partition coefficient found for the same test solute in a polar solvent. Rutan *et al.* [29] have argued that the above model may not account completely for all the details of the solvent reorganization process given that an *n*-alkane would probably not be as effective as a polar solute at disrupting the intermolecular bonding among solvent molecules. The cavity formation process, therefore, would be different for an *n*-alkane and a polar solute. At least three common models have been advanced that would allow the independent calculation of the Gibbs free energy of cavity formation based on the Hildebrand solubility parameter theory, scaled particle theory and Sinanoglu–Reis–Moura Ramos (SRMR) solvophobic theory [31,32]. However, it is difficult to see how these approaches could be applied to a diverse group of stationary phases with all the variations represented by polarity and size as well as the fact that most of the physical parameters required for the calculations are not available in the literature. In this paper we propose a new model to characterize solute–solvent polar interactions based on the general premise of linear solvation energy relationships and Snyder's treatment of the cavity/dispersion term. Multivariate analysis techniques are then applied to the size-independent free-energy interaction term to identify suitable test solutes for characterizing specific stationary phase polar interactions and to classify the stationary phases into clusters based on the similarity of their capacity for specific intermolecular interactions using a data set consisting of the partial molal Gibbs free energy of solution for 28 solutes on 23 stationary phases [17].

EXPERIMENTAL

The names, abbreviations and compositions of the 22 stationary phases and 25 test solutes used in this study are summarized in Table I. The data for the partial molal Gibbs free energy of solution for the test solutes at 121.4°C on each stationary phase are collected and summarized in ref. 17. The partial molal Gibbs free energy of solution for the *n*-alkanes on the phases used in this study were taken from several sources [3,8,9,33,34] and are summarized in Table II. The Van der Waals volume for the test solutes and *n*-alkanes were calculated by several methods. The Van der Waals volume according to Bondi, V_B, was calculated by summing the contribution of fragmental constants given by Bondi [35]. In a similar manner, the characteristic Van der Waals volume, V_X, was calculated from fragmental constants as described by McGowan [36,37] and Abraham and McGowan [38]. The intrinsic Van der Waals volume, V_I, introduced by Leahy [39] and Leahy *et al.* [40], was estimated in an approximate form using the correlation equation between the intrinsic and characteristic volume presented by Abraham and co-workers [38,41]. The Van der Waals volume, V_A, and Van der Waals total surface area and solvent accessible surface area were calculated with the molecular modeling program MacroModel version 2.0 (Department of Chemistry, Columbia University, New York) [42–44] executed on a VAX II/750 computer with version 4.7 of VMS (Digital Equipment, Merrimack, NH, USA). Multivariate analysis was performed on an Epson Apex 200 computer using Ein*Sight version 2.5 (Infometrix, Seattle, WA, USA) software for data analysis and pattern recgnition. The data were entered via a standard spreadsheet program, VP-

TABLE I

IDENTIFICATION AND ABBREVIATIONS FOR STATIONARY PHASES AND TEST SOLUTES

Stationary phases

No.	Abbreviation	Name
1	SE-30	Poly(dimethylsiloxane)
2	DDP	Didecyl phthalate
3	OV-105	Poly(cyanopropylmethyldimethylsiloxane)
4	OV-3	Poly(dimethylmethylphenylsiloxane), 10 mol% phenyl groups
5	OV-7	Poly(dimethylmethylphenylsiloxane), 20 mol% phenyl groups
6	OV-11	Poly(dimethylmethylphenylsiloxane), 35 mol% phenyl groups
7	OV-17	Poly(methylphenylsiloxane)
8	OV-22	Poly(methylphenyldiphenylsiloxane), 65 mol% phenyl groups
9	PPE-5	1,3-Bis(3-phenoxyphenoxy)benzene
10	OV-330	Poly(dimethylsiloxane)–Carbowax copolymer
11	QMES	Tetra-*n*-butylammonium 4-morpholinoethanesulfonate
12	OV-25	Poly(methylphenyldiphenylsiloxane), 75 mol% phenyl groups
13	CW20M	Poly(ethylene glycol)
14	QPIC	Tetra-*n*-butylammonium 4-picrate
15	QpTS	Tetra-*n*-butylammonium 4-toluenesulfonate
16	QF-1	Poly(trifluoropropylmethylsiloxane)
17	QACES	Tetra-*n*-butylammonium 2-(2-acetamido)aminoethanesulfonate
18	QTAPSO	Tetra-*n*-butylammonium 3-tris(hydroxymethyl)methylamino-2-hydroxy-1-propanesulfonate
19	DEGS	Poly(diethylene glycol succinate)
20	TCEP	1,2,3-Tris(2-cyanoethoxypropane)
21	OV-225	Poly(cyanopropylmethylphenylmethylsiloxane)
22	OV-275	Poly(dicyanoallylsiloxane)

Test solutes

No.	Name
1	Benzene
2	*n*-Butylbenzene
3	2-Methyl-2-pentanol
4	1-Nitropropane
5	1-Nitropentane
6	Nitrobenzene
7	Benzonitrile
8	Pyridine
9	2-Octanone
10	1,1,2,2-Tetrachloroethane
11	*n*-Butanol
12	*n*-Octanol
13	1-Dodecyne
14	Nonanal
15	1,4-Dioxane
16	Benzodioxane
17	N,N-Dimethylaniline
18	Anisole
19	Aniline
20	N-Methylaniline
21	2,6-Dimethylaniline
22	2-Octyne
23	*cis*-Hydrindane
24	Dihexyl ether
25	2,4,6-Trimethylpyridine

TABLE II

PARTIAL MOLAL GIBBS FREE ENERGY OF SOLUTON FOR *n*-ALKANES (kcal/mol) AT 121.4°C

Stationary phase	Hexane	Heptane	Octane	Nonane	Decane	Undecane	Dodecane	Tridecane	Tetradecane	Pentadecane
SQ			−3.944	−4.470	−4.991	−5.508	−6.026	−6.543		
OV-3				−3.756	−4.198	−4.671	−5.126	−5.577		
OV-7				−3.672	−4.140	−4.602	−5.065	−5.524		
OV-11				−3.528	−4.002	−4.464	−4.929	−5.390		
OV-17					−3.876	−4.345	−4.804	−5.260	−5.715	−6.169
OV-22					−3.674	−4.119	−4.563	−5.003	−5.444	−5.883
OV-25						−4.006	−4.436	−4.862	−5.312	−5.727
OV-105				−3.705	−4.155	−4.600	−5.043	−5.483	−5.922	
OV-225						−3.609	−3.998	−4.410	−4.822	−5.279
OV-375					−3.492	−3.921	−4.362	−4.789	−5.204	−5.638
QF-1					−3.147	−3.531	−3.915	−4.291	−4.668	−5.034
CW20M						−3.451	−3.812	−4.193	−4.592	−4.977
DEGS						−2.034	−2.226	−2.365	−2.828	−3.144
TCEP					−1.499	−1.935	−2.246	−2.548	−2.817	−3.037
PPE-5				−3.319	−3.803	−4.280	−4.756	−5.230		
QpTS						−3.325	−3.763	−4.079	−4.466	−4.772
QPIC						−3.326	−3.763	−4.155	−4.544	−4.942
QMES						−3.316	−3.712	−4.097	−4.368	−4.704
QACES						−2.350	−2.711	−2.713	−3.013	−3.321
QTAPSO						−1.857	−2.007	−2.318	−2.388	−2.581
DPP	−2.514	−3.059	−3.543	−4.071	−4.576	−5.081				
SE-30		−2.838	−3.323	−3.770	−4.224	−4.669	−5.122			

Planner, version 2.0 (Paperback Software International, Berkeley, CA, USA). Missing data points were added as described in ref. 17.

RESULTS AND DISCUSSION

In a previous study, multivariate analysis was applied to a collection of data in the form of the partial molal Gibbs free energy of solution for 28 test solutes on 23 stationary phases to identify suitable test solutes for the classification of stationary phases based on their capacity to enter into specific intermolecular interactions (dispersion, induction, orientation and proton donor–acceptor properties) [17]. For members of a homologous series, *e.g.*, Fig. 1, a good correlation was found between individual members of the series for the partial molal Gibbs free energy of solution except for a group of highly cohesive polar phases that behaved in a different manner to the other phases. This different behavior was speculated to result from the differences in the free energy of cavity formation for the two groups of stationary phases indicating that a more rigorous interpretation of the data was required to separate the contribution of solute size from terms describing the selective solute–solvent interactions that could be used as a basis for the classification of stationary phases.

If we assume that the total free energy change for the transfer of solute X from the gas phase to the stationary phase (with molecular interactions characteristic of infinite dilution) is the linear sum of the individual free energy contributions to the

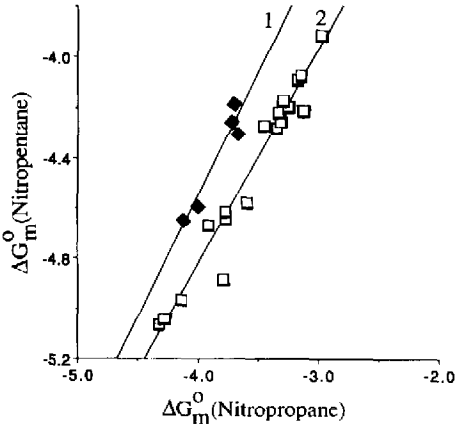

Fig. 1. Plot of the partial molal Gibbs free energy of solution for nitropentane against nitropropane for the stationary phases identified in Table I. Group 1 phases (DEGS, TCEP, QACES, QTAPSO, OV-275) are of high cohesive energy and are displaced from the remaining phases, Group 2, in the correlation plots.

transfer process, then a general expression for the solution process, can be written as follows:

$$\Delta G_S^{SOLN}(X) = \Delta G_S^{CAV}(X) + \Delta G_S^{NP}(X) + \Delta G_S^{P}(X) \quad (4)$$

where $\Delta G_S^{SOLN}(X)$ is the partial Gibbs free energy of solution for the transfer of solute X from the gas phase to the stationary phase S, $\Delta G_S^{CAV}(X)$ the partial Gibbs free energy of cavity formation for solute (X), $\Delta G_S^{NP}(X)$ the partial Gibbs free energy of interaction of the non-polar contribution of solute (X) with the surrounding solvent and $\Delta G_S^{P}(X)$ the partial Gibbs free energy of interaction for the polar contribution of solute (X) with the surrouding solvent. The cavity term is a measure of the free energy required to separate the solvent molecules to create a cavity of a suitable size to hold the solute. It depends only on the size of the solute and the strength of intermolecular interactions between the solvent molecules. However, the independent calculation of the cavity term is not a simple task and requires the input of solvent parameters that are largely unavailable for the stationary phases employed in this study [31,32]. Also, there are no suitable methods that enable either ΔG_S^{NP} or ΔG_S^{P} to be calculated directly. A practical solution can be found if a few simplifying assumptions are made. The polar contribution of the free energy of solution of solute (X) is assumed to be equal to the difference between the free energy of solution of solute (X) in stationary phase S and the free energy of solution for a hypothetical *n*-alkane with an identical molecular volume in the same stationary phase. Thus,

$$\Delta G_S^{SOLN}(HC)^{V} = \Delta G_S^{CAV}(X) + \Delta G_S^{NP}(X) \quad (5)$$

and the difference between eqns. 4 and 5 provides a value for $\Delta G_S^{P}(X)$ in terms of experimentally derived values:

$$\Delta G_S^{P}(X) = \Delta G_S^{SOLN}(X) - \Delta G_S^{SOLN}(HC)^{V} \quad (6)$$

where $(HC)^V$ identifies a parameter representing a property of an *n*-alkane with a volume V identical with that of solute (X). An exact value for $\Delta G_S^{SOLN}\ (HC)^V$ can be obtained by linear regression from a plot of the partial molal Gibbs free energy of solution for a series of *n*-alkanes against their molecular volume. The induction component to $\Delta G_S^P\ (X)$ can be removed by assuming that this equivalent to the polar contribution to the free energy of solution of solute (X) in a non-polar hydrocarbon solvent, such as squalane. This can be calculated in a manner similar to solvent S and is given by

$$\Delta G_{SQ}^P\ (X) = \Delta G_{SQ}^{SOLN}\ (X) - \Delta G_{SQ}^{SOLN}\ (HC)^V \tag{7}$$

The solvent interaction term for polar interactions can then be formally defined as

$$\Delta G_S^{INT}\ (X) = \Delta G_S^P\ (X) - \Delta G_{SQ}^P\ (X) \tag{8}$$

and is equivalent to the solute solvent interactions of solute (X) that exceed those interactions typified by an *n*-alkane of identical molecular volume in solvent S reduced by the identical interactions of solute (X) in a hydrocarbon solvent (SQ). The partial Gibbs free energy contributions to solution from cavity formation, dispersion, induction and reorganization entropy changes should be largely eliminated making $\Delta G_S^{INT}\ (X)$ the most logical term to probe the importance of solute orientation and hydrogen-bonding interactions. It should be noted that during the above discussion no mention was made of the standard state for the solution. As differences in free energies are involved, which are proportional to differences in logarithmic terms, all constants for the standard state (molarity, mole fraction or molality) are self-cancelling, resulting in identical numerical values for $\Delta G_S^{INT}\ (X)$. All absolute values for free energies of solution are quoted as the partial molal Gibbs free energy of solution in this paper.

The electron cloud surrounding the nucleus of an atom has no clearly defined boundary surface and consequently, an atom has no absolute volume [45,46]. From studies in interatomic bonding an empirical volume, the Van der Waals volume, has been widely used to describe the size of atoms and molecules in studies of their physical properties. In the Van der Waals volume concept each atom of a molecule is represented as a sphere centered at the equilibrium position of the atomic nucleus and having a radius equal to the Van der Waals radius of the atom. The Van der Waals surface can be defined as the exterior surface of the union of all such Van der Waals spheres in the molecule. Clearly the Van der Waals surface and hence volume of a molecule will depend on the empirically based choice of the atomic Van der Waals radii. The simplest approach for approximating the Van der Waals volume of a molecule is to add up appropriate chemical group contributions (increments) using tabulated atomic volumes such as those proposed by Bondi [35]. Such table-based methods can only address in an approximate manner multiple overlaps of atomic Van der Waals spheres in complex molecules and isomers. Empirical force field methods (molecular mechanics) have advanced to a level where accurate geometries, and therefore volumes, can be obtained for most simple organic structures. Differences between methods can be expected, however, owing to differences in force-field approximations and the selected empirical atomic radii. The intrinsic volume of Leahy *et al.* is one example of a widely used approach to predicting molecular volumes [39–41]. In this study we used the program MacroModel [42–44] to calculate molecular volumes

which takes a similar approach to that of Leahy *et al.*, but is not necessarily identical with it. McGowan also proposed a characteristic volume for a molecule that is calculated from considerations of parachor [36,37]. The characteristic volume is defined as the volume of 1 mole of liquid when the molecules are not in motion (absolute zero) and, like the method of Bondi, has the advantage that molecular volumes can be simply built up by addition of atomic values followed by subtraction of a fixed constant for each bond regardless of hybridization. Characteristic volumes are larger than Van der Waals volumes calculated by Bondi methods or molecular mechanics. Abraham and co-workers [38,41] have shown that there is a very good correlation between the computer-calculated intrinsic volume (V_I) and McGowans characteristic volume (V_X):

$$V_I = 0.597 + 0.6823\ V_X \qquad r = 0.99;\ n = 209 \tag{9}$$

The molar volume has also been widely used to correlate the size of a molecule with intrinsic physical properties and is easily calculated from the molecular weight and density of a substance. However, the molar volume has certain theoretical disadvantages compared with the Van der Waals volume [38–41]. The molar volume is a bulk property conditioned by the strength of intermolecular interactions and its magnitude reflects not only the intrinsic volume of the molecule but also its bulk structure. In solute–solvent interactions correlations involving the molar volume result in an underestimate of the contribution of polar interactions which have to be empirically corrected for by modifying the cavity term. Thus the molar volume was considered a poor choice compared with the Van der Waals volume for the purpose of our studies. However, the question remained of how to select the most appropriate Van der Waals volume from the several methods available for its calculation.

The Van der Waals volumes calculated according to Bondi [35], V_B, McGowan [35,37] and Abraham and McGowan [38], V_X, from the MacroModel program, V_A, and the intrinsic volume, V_I, estimated by eqn. 9 and compared with literature values [39–41] are summarized in Table III. The characteristic volume is considerably larger than the other estimates of the Van der Waals volume but is linearly correlated with the intrinsic volume [38] (eqn. 9) and with the Bondi volume (eqn. 10) and the MacroModel calculated volume (eqn. 11):

$$V_I = -0.38 + 0.72\ V_B \qquad r = 1.00;\ n = 35 \tag{10}$$

$$V_I = -1.14 + 0.73\ V_A \qquad r = 1.00;\ n = 35 \tag{11}$$

Likewise, the Bondi volume and the computed volume using the MacroModel program are very similar numerically (Table III) and are correlated:

$$V_B = 0.60 + 1.01\ V_A \qquad r = 1.00;\ n = 35 \tag{12}$$

There are absolute differences between the computed intrinsic volumes calculated by Leahy [39] and those obtained using the MacroModel program, which in general produces values similar to those of Bondi [35]. Differences between V_A and V_B are due to allowance for deviations from a hard-sphere volume caused by overlap in the computer calculated volumes. Because of the good correlations between individual methods for calculating Van der Waals volumes, the choice of method in the relative sense is not too important as any differences between individual methods reflect only

TABLE III

VAN DER WAALS VOLUMES AND SURFACE AREAS CALCULATED BY DIFFERENT METHODS

Test solute	Van der Waals volume (cm^3/mol)					Surface area (Å^2)	
	Characteristic, V_X	Intrinsic, V_I		Bondi, V_B	MacroModel, V_A	Total	Solvent Accessible[a]
		Estm.	Calc.				
Dioxane	68.1	46.5		49.00	52.99	114.1	184.1
Butanol	73.1	49.9	49.9	52.65	53.42	124.3	180.2
Nitropropane	70.6	48.2		50.83	49.32	125.5	214.7
Nitropentane	98.7	67.3		71.33	69.61	170.6	258.6
Nitrobenzene	89.1	60.8	63.1	64.33	61.61	138.8	206.5
Octanol	129.5	88.4	88.2	93.81	94.79	215.6	269.3
Benzodioxane	107.3	73.2		77.58	72.81	152.2	201.2
Dihexyl ether	185.8	126.8		134.90	135.56	304.7	407.8
Benzene	71.6	48.9	49.1	51.56	50.46	106.7	159.9
Butylbenzene	128.0	87.3		92.72	92.72	194.4	245.3
cis-Hydrindane	116.0	79.1		83.92	85.15	142.8	251.3
2-Octyne	115.0	78.5		83.21	81.84	182.5	264.8
1-Dodecyne	171.3	116.9		124.34	122.79	278.2	371.1
2-Methyl-2-pentanol	101.3	69.1		73.21	73.59	164.3	213.0
Benzonitrile	87.1	59.4	59.0	62.87	61.30	124.3	178.8
Tetrachloroethane	86.9	59.3	61.7	62.74	65.28	132.3	224.1
Pyridine	67.5	46.1		48.58	47.75	98.2	153.6
Trimethylpyridine	109.8	74.9		79.43	77.44	161.2	220.1
Aniline	81.6	55.7		58.87	57.03	113.9	163.1
N-Methylaniline	95.7	65.3		69.15	67.15	139.1	193.2
N,N-Dimethylaniline	109.8	74.9	75.2	79.43	78.29	162.0	215.7
2,6-Dimethylaniline	109.8	74.9		79.43	77.02	156.1	197.7
Anisole	91.6	62.5	63.0	66.15	64.86	138.7	189.3
Nonanal	139.2	95.0		100.92	99.85	234.6	284.5
2-Octanone	125.2	85.4		90.64	88.58	210.2	277.5
Butane	67.2	45.9		47.80	47.88	115.1	193.8
Pentane	81.3	55.5	55.3	58.03	57.99	138.7	223.9
Hexane	95.4	65.1	64.8	68.26	68.29	161.9	240.7
Heptane	109.5	74.7	74.5	78.49	78.35	184.9	269.0
Octane	123.6	84.3	84.2	88.72	88.76	206.4	280.5
Nonane	137.7	93.9		98.85	98.88	229.4	300.9
Decane	151.8	193.5		109.18	109.12	248.5	343.3
Undecane	165.9	113.2		119.41	119.48	274.2	368.1
Dodecane	179.9	122.8		129.64	130.08	296.8	392.9
Tridecane	194.0	132.4		139.87	139.59	320.4	411.5

[a] Calculated for water as solvent.

subtle changes in volumes which will not have a significant impact on the final results calculated using eqn. 6. For calculations using the Van der Waals volume in this paper we adopted the volume, V_A, calculated by the MacroModel program.

As molecules interact at their surfaces, the cavity surface area might be more appropriate than the cavity volume for accessing the ability of a solute to interact with surrouding solvent molecules [43,45–47]. The Van der Waals surface area is

defined as the surface of the intersection of all Van der Waals spheres in a molecule and is often referred to as the total surface area (*TSA*) (Table III). The total surface area is correlated with the Van der Waals volume:

$$V_A = 0.70\,(TSA) + 7.34 \qquad r = 0.99;\ n = 35 \tag{13}$$

although in this case individual molecular variations are much greater than was observed for the different volume terms (Fig. 2). The total surface area may reveal subtle structural features not apparent in the volume term but should not lead to gross differences in the computation of the solvent interaction terms. As the dimensions of molecules are always finite compared with the dimensions over which they interact, the total surface area may not be the most appropriate parameter for gauging solute–solvent interactions [45,46,48]. A solvent-accessible surface area can be defined as the locus of the center of a solvent sphere of fixed radius as it is rolled over the Van der Waals surface of the solute. The accessible surface area is directly related to the number of solvent molecules which could be packed around the solute and is thus indirectly related to the energy of solute–solvent interactions. However, as the choice of solvent radius is ill-defined, it has been suggested that the contact surface area could be a better alternative to the solvent-accessible area. The contact surface area is defined as those parts of the Van der Waals surface that can actually make contact with the surface of the probe. Unfortunately, both the solvent–accessible and contact surface areas require a detailed knowledge of the solvent molecules, which would be difficult for us to compute given the wide range of solvent types and size represented by the stationary phases listed in Table I. For comparative purposes we have computed the solvent-accessible surface area of the test solutes for water as solvent (spherical radius 1.4 Å), which are listed in Table III. There is generally only a poor correlation between the solvent–accessible surface area and the total surface area (for water $r = 0.97$, $n = 35$) or molecular volume, V_A (for water $r = 0.95$, $n = 35$), indicating that whereas substituting the total surface area for the molecular

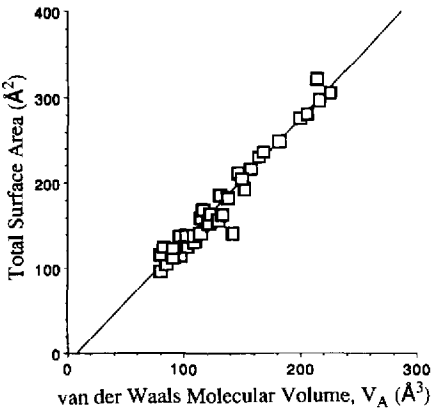

Fig. 2. Plot of the Van der Waals total surface area against the Van der Waals volume, V_A, for the 35 test solutes identified in Table III.

volume would only fine tune the solvent selectivity calculations, the use of the solvent–accessible or contact surface area could significantly modify the predictions obtained. However, the calculation of the solvent-accessible and contact areas is not a trivial task and exceeds our current capabilities for molecular modeling.

In the remaining portion of this paper the Van der Waals volume, V_A, has been used as the basis for the correction term to eliminate the influence of solute size on the solvent selectivity parameter. This is done through the solvent polar interaction parameter (eqn. 6), by subtracting from the partial Gibbs free energy of solution for the equivalent free energy of solution for a hypothetical *n*-alkane with an identical Van der Waals volume. The numerical value of the polar contribution to the free energy of solution corresponds to

$$\Delta G_S^P (X) = -2.303\, RT \log (K_L^X / K_L^{n^V}) \tag{14}$$

where K_L^X is the gas–liquid partition coefficient for solute (X) and $K_L^{n^V}$ is the gas–liquid partition coefficient for a hypothetical *n*-alkane with an identical Van der Waals volume to solute (X). Values for the latter are simply obtained from the linear relationship between log K_L^{alkane} and the Van der Waals volume:

$$\log K_L^{alkane} = m_S\, V_A\, (\text{alkane}) + b_S \tag{15}$$

where m_S and b_S are the solvent-dependent regression coefficients summarized in Table IV. The limiting factor for the accurate determination of m_S and b_S is the

TABLE IV

REGRESSION COEFFICIENTS AND CORRELATION COEFFICIENTS FOR USE WITH EQN. 15

Stationary Phase	m_S	b_S	r
Squalane	0.0281	−0.5519	1.00
OV-3	0.0247	−0.5313	1.00
OV-7	0.0251	−0.5813	1.00
OV-11	0.0252	−0.6420	1.00
OV-17	0.0249	−0.6609	1.00
OV-22	0.0240	−0.6670	1.00
OV-25	0.0234	−0.6496	1.00
OV-105	0.0240	−0.4791	1.00
OV-225	0.0227	−0.8199	1.00
OV-275	0.0144	−1.4185	0.91
OV-330	0.0233	−0.6978	1.00
QF-1	0.0204	−0.5132	1.00
CW20M	0.0217	−0.7959	1.00
DEGS	0.0156	−0.8136	0.99
TCEP	0.0152	−0.8589	0.99
PPE-5	0.0260	−0.7931	1.00
QpTS	0.0199	−0.6247	1.00
QPIC	0.0215	−0.7857	1.00
QMES	0.0188	−0.4994	1.00
QACES	0.0126	0.2860	0.99
QTAPSO	0.0091	−0.1254	0.98
DPP	0.0277	−0.6585	1.00
SE-30	0.0244	−0.5263	1.00

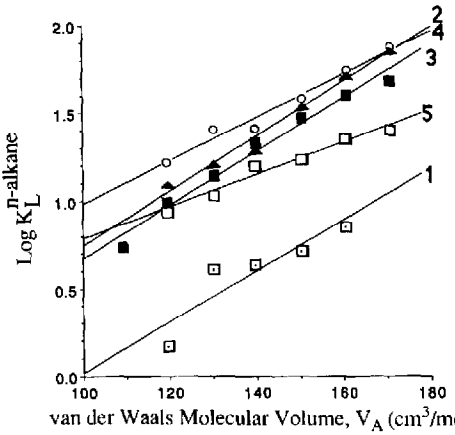

Fig. 3. Plot of the logarithm of the gas–liquid partition coefficient for *n*-alkanes against the Van der Waals volume, V_A, for the stationary phases of high cohesive energy. 1 = OV-275; 2 = DEGS; 3 = TCEP; 4 = QACES; 5 = QTAPSO.

relative magnitude of K_L^{alkane}, which depends on the solubility of the *n*-alkane in the solvent. On the most polar phases *n*-alkanes are retained largely by interfacial adsorption resulting in very small gas–liquid partition coefficients [2,3,8,9]. Log K_L^{alkane} as a function of the Van der Waals volume for the most cohesive phases, the worse case situation, are shown in Fig. 3. The data seems reasonable for DEGS, TCEP, QACES and QTAPSO, but for OV-275 the scatter is too great to believe that the coefficients m_S and b_S in Table IV are any more than roughly determined for this phase.

As an alternative to eqn. 7, it was considered that the cavity and non-polar interaction term might be approximated by

$$\Delta G^{CAV} + \Delta G^{NP} = [V_A/V_{(CH_2)}]\,\Delta G^{CH_2} \tag{16}$$

where $V_{(CH_2)}$ is the van der Waals volume of a methylene group and ΔG^{CH_2} the partial Gibbs free energy of solution for a methylene group. ΔG^{CH_2} can be determined from the periodic change in free energy for any homologous series, such as 2-alkanones, which have much larger gas–liquid partition coefficients on polar phases and show good linear correlations for plots similar to Fig. 3, even for OV-275 [8,9]. However, this approach leads to an overestimate of the left-hand term in eqn. 16 and positive Gibbs free energy of solution values for *n*-alkanes and other non-polar solutes on several phases, which, of course, are theoretically impossible. A plot of the partial molal Gibbs free energy of solution for homologous *n*-alkanes and 2-alkanones as a function of the Van der Waals volume on two different phases is shown in Fig. 4. The intercept term corresponding to the transfer of a solute of zero van der Waals volume is substantial, and further depends on both the identities of the solute and the solvent. This prevents any simple correction term being developed to modify eqn. 16 for its overestimate of the free-energy term. The physical significance of the intercept and its dependence on the identities of the solute and the solvent is not clear. Others have speculated on similar or related findings, but their arguments are not very convincing [26,27,45,46].

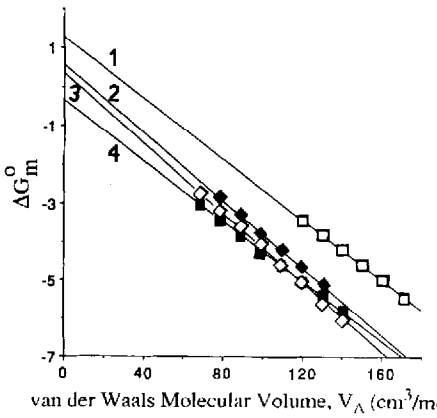

Fig. 4. Plot of the partial molal Gibbs free energy of solution for *n*-alkanes (1 and 2) and 2-alkanones (3 and 4) on SE-30 (2 and 3) and CW20M (1 and 4).

TABLE V

PARTIAL GIBBS FREE ENERGY OF SOLUTION FOR CAVITY FORMATION AND NON-POLAR INTERACTIONS ($\Delta G^{CAV} + \Delta G^{NP}$) AND POLAR INTERACTIONS (ΔG^P) ON THE HYDROCARBON STATIONARY PHASE SQUALANE

Test Solute	$\Delta G^{CAV} + \Delta G^{NP}$ (kcal/mol)	ΔG^P (kcal/mol)
Benzene	−2.004	−1.156
n-Butylbenzene	−4.058	−1.151
Dihexyl ether	−6.322	−0.044
cis-Hydrindane	−3.713	−1.317
2-Octyne	−3.596	−0.564
1-Dodecyne	−5.674	−0.276
Nonanal	−4.510	−0.675
Dioxane	−2.133	−1.011
Benzodioxane	−3.138	−2.367
N,N-Dimethylaniline	−3.416	−1.877
Anisole	−2.734	−1.636
2,4,6-Trimethylpyridine	−3.373	−1.417
2-Octanone	−3.938	−0.676
1,1,2,2-Tetrachloroethane	−2.756	−1.569
Butanol	−2.154	−0.557
Octanol	−4.253	−0.716
2-Methyl-2-pentanol	−3.178	−0.138
Nitropropane	−1.946	−1.195
Nitropentane	−2.976	−1.241
Nitrobenzene	−2.569	−2.486
Benzonitrile	−2.554	−1.907
Pyridine	−1.867	−1.534
Aniline	−2.337	−2.132
N-Methylaniline	−2.851	−2.185
2,6-Dimethylaniline	−3.352	−2.223

Returning to eqn. 7 and considering the polar interaction term for the test solutes on the hydrocarbon stationary phase squalane (Table V), the polar interaction term characterizes the partial Gibbs free energy of solution which exceeds those interactions of an *n*-alkane of identical Van der Waals volume, and in the case of the hydrocarbon squalane is expected to arise primarily from induction interactions since orientation and proton donor–acceptor interactions should be absent. In all cases ($\Delta G_{SQ}^{CAV} + \Delta G_{SQ}^{NP}$) is greater than ΔG_{SQ}^{P}, which would be expected for squalane. For the homologous test solutes benzene–*n*-butylbenzene, butanol–octonal and nitropropane–nitropentane, the values for ΔG_{SQ}^{P} are very similar, which would be predicted if the estimates of $\Delta G_{SQ}^{CAV} + \Delta G_{SQ}^{NP}$ were realistic. Similarly, the magnitude of ΔG_{SQ}^{P} for the non-polar solutes dihexyl ether, 2-octyne, 1-dodecyne, nonanal and 2-octanone are small with respect to the magnitude of $\Delta G_{SQ}^{CAV} + \Delta G_{SQ}^{NP}$ in agreement with intuition. On the other hand, ΔG_{SQ}^{P} values seem relatively too large for all the aromatic solutes and *cis*-hydrindane, for example, benzene has $\Delta G_{SQ}^{CAV} + \Delta G_{SQ}^{NP} = -2.004$ kcal/mol and $\Delta G_{SQ}^{P} = -1.156$ kcal/mol. It would seem likely that the hardcore Van der Waals volumes are a poor estimate of the size of the cavity and its accessible surface for solvent interactions for aromatic and cyclic solutes. This is part of the justification for referencing ΔG_{S}^{INT} (X) to ΔG_{SQ}^{P} (X) in the hope of correcting, at least partially, for the non-polar contribution to ΔG_{S}^{P} (X) not accounted for by $\Delta G_{S}^{CAV} + \Delta G_{S}^{NP}$ owing to an incorrect estimate of the solvent–accessible cavity surface by the Van der Waals volume for cyclic and aromatic solutes. The other reason is to remove from the solvent interaction term the solute induction contribution to ΔG_{S}^{P} (X). For the solutes with large dipole moments in Table V this contribution is far from negligible.

The sum of $\Delta G_{S}^{CAV} + \Delta G_{S}^{NP}$ for 25 solutes on 21 stationary phases is summarized in Table VI. The cavity term is endoergic and of opposite sign to the nonpolar partial Gibbs free energy of solution term. All values of $\Delta G_{S}^{CAV} + \Delta G_{S}^{NP}$ are negative and increase in magnitude with the size of the solute. For any particular solute the magnitude of the term $\Delta G_{S}^{CAV} + \Delta G_{S}^{NP}$ decreases with increasing solvent strength, in reasonable agreement with the order predicted by the solvent strength parameter [3,8]. To a first approximation, solutes of the same size will have similar contributions from dispersion to the $\Delta G_{S}^{CAV} + \Delta G_{S}^{NP}$ term. For an individual solute the descending order of the $\Delta G_{S}^{CAV} + \Delta G_{S}^{NP}$ term should be roughly proportional to the cavity term, the free energy required to create a hole in the solvent of a certain size by breaking solvent–solvent bonds. This is borne out by multivariate analysis of the data in Table VI, which indicates that 98.6% of the total variance in the data is accounted for by one component vector. The lowest correlation coefficient for any two solutes on all stationary phases in Table VI is $r = 0.90$ (2,4,6-trimethylpyridine *vs.* dihexyl ether) and most values exceed $r = 0.99$. Thus, it can be concluded that $\Delta G_{S}^{CAV} + \Delta G_{S}^{NP}$ is independent of the identity of the solute, except for its size, and is independent of the magnitude of solute-solvent polar interactions. The relative magnitude of $\Delta G_{S}^{CAV} + \Delta G_{S}^{NP}$ indicates that as solute size increases the term becomes more favorable for transfer from the gas phase as ΔG_{S}^{NP} (X) grows faster in importance than the opposing contribution from ΔG_{S}^{CAV} (X). However, the more cohesive the solvent, the less favorable is the cavity term for the transfer from the gas phase and the term, $\Delta G_{S}^{CAV} + \Delta G_{S}^{NP}$ is always less favorable for solvents of high cohesive energy (that is, solvents with a propensity for significant solvent–solvent polar interactions) than for solvents

TABLE VI

CONTRIBUTIONS FROM CAVITY AND NON-POLAR INTERACTION TERMS TO THE SOLUTION OF TEST SOLUTES IN STATIONARY PHASES OF DIFFERENT POLARITY (kcal/mol)

Stationary phase	Benzene	*n*-Butylbenzene	Dihexyl ether	*cis*-Hydrindane	2-Octyne	2-Methyl-2-pentanol	Nitropropane	Nitropentane	Nitrobenzene
SE-30	−1.880	−3.663	−5.629	−3.364	−3.262	−2.898	−1.829	−2.723	−2.370
DPP	−1.643	−3.667	−5.899	−3.328	−3.212	−2.800	−1.586	−2.601	−2.200
OV-105	−1.612	−3.366	−5.300	−3.072	−2.972	−2.614	−1.562	−2.442	−2.095
OV-3	−1.586	−3.391	−5.382	−3.089	−2.986	−2.618	−1.535	−2.440	−2.083
OV-7	−1.489	−3.323	−5.345	−3.015	−2.911	−2.537	−1.437	−2.357	−1.994
OV-11	−1.333	−3.175	−5.205	−2.866	−2.761	−2.385	−1.281	−2.205	−1.840
OV-17	−1.254	−3.074	−5.080	−2.769	−2.665	−2.294	−1.203	−2.115	−1.755
OV-22	−1.141	−2.894	−4.828	−2.600	−2.500	−2.143	−1.091	−1.971	−1.623
PPE-5	−1.041	−2.941	−5.036	−2.622	−2.514	−2.127	−0.987	−1.940	−1.564
OV-225	−0.764	−2.423	−4.252	−2.145	−2.050	−1.712	−0.717	−1.549	−1.221
OV-330	−1.034	−2.736	−4.614	−2.451	−2.354	−2.006	−0.985	−1.839	−1.502
QMES	−1.017	−2.391	−3.905	−2.160	−2.082	−1.802	−0.978	−1.667	−1.395
OV-25	−1.084	−2.794	−4.679	−2.507	−2.409	−2.061	−1.035	−1.893	−1.554
CW20M	−0.705	−2.291	−4.039	−2.025	−1.934	−1.611	−0.660	−1.455	−1.142
QPIC	−0.673	−2.244	−3.976	−1.980	−1.891	−1.570	−0.628	−1.416	−1.105
QpTS	−0.876	−2.330	−3.934	−2.087	−2.004	−1.707	−0.835	−1.564	−1.276
QF-1	−1.003	−2.494	−4.138	−2.244	−2.159	−1.855	−0.961	−1.709	−1.414
QACES	−0.806	−1.727	−2.742	−1.572	−1.520	−1.332	−0.780	−1.242	−1.059
QTAPSO	−0.755	−1.420	−2.153	−1.309	−1.271	−1.135	−0.736	−1.070	−0.938
DEGS	−0.014	−1.153	−2.410	−0.962	−0.897	−0.665	−0.019	−0.553	−0.327
TCEP	−0.004	−1.115	−2.340	−0.929	−0.865	−0.639	−0.027	−0.530	−0.310

	Benzonitrile	Pyridine	2,4,6-Trimethylpyridine	2-Octanone	1,1,2,2-Tetrachloroethane	Butanol	Octanol	1-Dodecyne
SE-30	−2.357	−1.760	−3.068	−3.559	−2.532	−2.020	−3.832	−5.066
DPP	−2.185	−1.507	−2.992	−3.550	−2.384	−1.790	−3.860	−5.260
OV-105	−2.082	−1.495	−2.781	−3.264	−2.254	−1.740	−3.533	−4.746
OV-3	−2.070	−1.465	−2.790	−3.287	−2.247	−1.718	−3.563	−4.812
OV-7	−1.980	−1.366	−2.711	−3.216	−2.160	−1.622	−3.497	−4.767

OV-11	−1.826	−1.210	−2.561	−3.068	−2.007	−1.467	−3.350	−4.624
OV-17	−1.742	−1.132	−2.467	−2.968	−1.920	−1.387	−3.247	−4.506
OV-22	−1.610	−1.023	−2.310	−2.793	−1.783	−1.269	−3.061	−4.275
PPE-5	−1.550	−0.914	−2.308	−2.831	−1.736	−1.179	−3.122	−4.436
OV-225	−1.209	−0.653	−1.870	−2.327	−1.372	−0.885	−2.581	−3.729
OV-330	−1.490	−0.920	−2.169	−2.637	−1.657	−1.158	−2.898	−4.076
QMES	−1.385	−0.925	−1.933	−2.311	−1.520	−1.117	−2.521	−3.472
OV-25	−1.542	−0.969	−2.224	−2.694	−1.710	−1.208	−2.956	−4.140
CW20M	−1.130	−0.599	−1.762	−2.199	−1.285	−0.821	−2.442	−3.539
QPIC	−1.093	−0.567	−1.720	−2.153	−1.248	−0.787	−2.393	−3.480
QpTS	−1.266	−0.779	−1.846	−2.246	−1.408	−0.982	−2.469	−3.475
QF-1	−1.402	−0.903	−1.997	−2.407	−1.549	−1.112	−2.636	−3.667
QACES	−1.053	−0.744	−1.420	−1.673	−1.143	−0.873	−1.814	−2.451
QTAPSO	−0.933	−0.711	−1.199	−1.382	−0.999	−0.804	−1.484	−1.944
DEGS	−0.319	−0.063	−0.774	−1.087	−0.431	−0.097	−1.262	−2.051
TCEP	−0.302	−0.070	−0.745	−1.051	−0.411	−0.085	−1.221	−1.989

	Nonanal	Dioxane	Benzodioxane	N,N-Dimethylaniline	Anisole	Aniline	N-Methylaniline	2,6-Dimethylaniline
SE-30	−4.055	−1.991	−2.864	−3.105	−2.514	−2.169	−2.614	−3.050
DPP	−4.113	−1.769	−2.760	−3.034	−2.363	−1.971	−2.477	−2.971
OV-105	−3.752	−1.722	−2.580	−2.818	−2.236	−1.896	−2.335	−2.763
OV-3	−3.789	−1.699	−2.583	−2.827	−2.228	−1.879	−2.330	−2.771
OV-7	−3.727	−1.603	−2.501	−2.750	−2.141	−1.786	−2.245	−2.692
OV-11	−3.580	−1.448	−2.350	−2.599	−1.988	−1.632	−2.092	−2.542
OV-17	−3.474	−1.368	−2.259	−2.505	−1.901	−1.549	−2.004	−2.448
OV-22	−3.281	−1.250	−2.109	−2.346	−1.764	−1.425	−1.864	−2.292
PPE-5	−3.359	−1.160	−2.090	−2.347	−1.717	−1.349	−1.824	−2.288
OV-225	−2.788	−0.868	−1.680	−1.905	−1.354	−1.033	−1.448	−1.853
OV-330	−3.111	−1.140	−1.974	−2.204	−1.639	−1.310	−1.735	−2.151
QMES	−2.693	−1.103	−1.775	−1.961	−1.505	−1.240	−1.583	−1.918
OV-25	−3.170	−1.190	−2.028	−2.259	−1.692	−1.361	−1.788	−2.206
CM20M	−2.640	−0.804	−1.580	−1.795	−1.269	−0.962	−1.359	−1.746
QPIC	−2.590	−0.771	−1.540	−1.753	−1.231	−0.927	−1.320	−1.704
QpTS	−2.651	−0.967	−1.679	−1.876	−1.393	−1.112	−1.476	−1.830
QF-1	−2.822	−1.096	−1.826	−2.028	−1.533	−1.245	−1.618	−1.981
QACES	−1.929	−0.863	−1.314	−1.439	−1.133	−0.955	−1.185	−1.410
QTAPSO	−1.567	−0.797	−1.122	−1.212	−0.992	−0.863	−1.029	−1.192
DEGS	−1.405	−0.085	−0.643	−0.797	−0.419	−0.198	−0.483	−0.762
TCEP	−1.360	−0.074	−0.618	−0.768	−0.399	−0.184	−0.462	−0.733

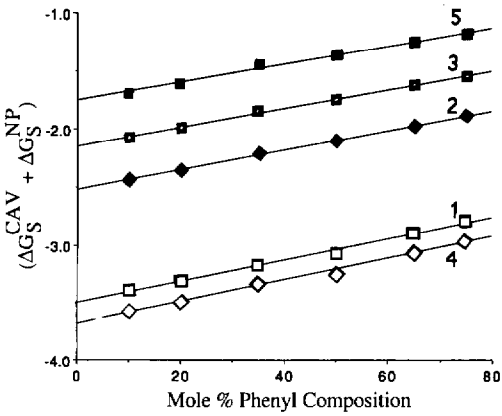

Fig. 5. Plot of $\Delta G_S^{CAV} + \Delta G_S^{NP}$ against mole percentage phenyl composition for a homologous series of poly(methylphenyl)siloxane solvents. 1 = *n*-butylbenzene; 2 = nitropentane; 3 = nitrobenzene; 4 = octanol; 5 = dioxane.

of low cohesive energy. For the homologous series of poly(methylphenyl)siloxanes varying in mole percentage phenyl composition there is a linear decrease in $\Delta G_S^{CAV} + \Delta G_S^{NP}$ with increasing mole percentage phenyl, which is independent of the solute identity (Fig. 5). The linear behavoir supports the view that changes in $\Delta G_S^{CAV} + \Delta G_S^{NP}$ are due to the cavity term, which depends on solvent–solvent interactions only.

The polar interaction term ΔG_S^{INT} (X) for 25 solutes on 21 phases is summarized in Table VII. ΔG_S^{INT} (X) should have values from zero to negative numbers representing solute–solvent interactions that are favorable to the solution process. This is generally the case. A few positive values are observed for weakly selective phase such as SE-30 and/or weakly selective test solutes such as *cis*-hydrindane. In most instances these values are very small and could simply be dismissed as resulting from experimental error [3]; however, as discussed previously for squalane, there may also be a contribution from ΔG_S^{NP} (X) caused by a poor approximation of the solvent-accessible cavity surface by a Van der Waals volume which is only roughly cancelled out by referencing the interactions to those in a hydrocarbon solvent (squalane). This would be particularly true for test solutes such as *cis*-hydrindane. ΔG_S^{INT} (X) should also be independent of solute size for homologous compounds. In Fig. 1 it was shown that of a plot of the partial molal Gibbs free energy of solution for nitropentane against nitropropane did not yield a single correlation with phases of high cohesive energy behaving anomalously compared with the weaker solvents. Fig. 6 shows the behavior for a plot of ΔG_S^{INT} (X) for nitropentane against nitropropane. The highly cohesive phases are no longer behaving anomalously (r = 1.00). The slope, 0.99, is very close to 1.00 and the intercept, −6.77 cal/mol, near zero, indicating that the influence of solute size on the magnitude of polar solute–solvent interactions has been effectively removed. The relevant data for the other homologous solutes are butylbenzene–benzene (r = 0.99, slope = 0.96 and intercept = 43 cal/mol) and octanol–butanol (r = 0.99, slope = 1.06 and intercept = 153.6 cal/mol). For the homologous series of poly(methylphenyl)siloxane solvents, replacing phenyl by methyl should, ignoring secondary interactions as the relative concentration of phenyl groups in-

TABLE VII

CALCULATED VALUES OF ΔG_s^{INT}(X)(kcal/mol)

Stationary phase	Benzene	Butylbenzene	2-Methyl-2-pentanol	1-Nitropropane	1-Nitropentane	Nitrobenzene
OV-3	−0.064	−0.045	−0.272	−0.424	−0.402	−0.252
OV-7	−0.173	−0.154	−0.349	−0.626	−0.609	−0.513
OV-11	−0.303	−0.302	−0.429	−0.857	−0.821	−0.797
OV-17	−0.283	−0.381	−0.467	−0.956	−0.925	−0.947
OV-22	−0.454	−0.478	−0.571	−1.055	−1.014	−1.080
OV-25	−0.580	−0.558	−0.513	−1.076	−1.047	−1.141
OV-105	0.026	0.023	−0.294	−0.418	−0.419	−0.182
OV-225	−1.156	−1.151	−0.138	−1.195	−1.241	−2.486
OV-330	−0.711	−0.685	−1.204	−1.600	−1.539	−1.694
QF-1	−0.105	−0.130	−0.680	−1.316	−1.329	−0.945
CW20M	−1.060	−0.960	−1.582	−2.079	−1.981	−2.294
DEGS	−1.308	−1.409	−2.147	−2.501	−2.518	−2.746
TCEP	−1.546	−1.505	−2.294	−2.965	−2.886	−3.020
PPE-5	−0.786	−0.755	−0.901	−1.427	−1.404	−1.671
QpTS	−0.841	−0.816	−2.359	−2.295	−2.264	−2.480
QPIC	−1.091	−1.038	−1.604	−2.318	−2.315	−2.466
QMES	−0.668	−0.731	−2.347	−2.126	−2.139	−2.336
QACES	−0.584	−0.779	−2.267	−2.035	−2.116	−2.372
QTAPSO	−0.476	−0.791	−2.054	−1.796	−1.956	−2.159
DPP	−0.409	−0.366	−0.666	−1.027	−1.051	−1.100
SE-30	0.092	0.103	−0.143	−0.129	−0.122	0.088

	Benzonitrile	Pyridine	2-Octanone	1,1,2,2-Tetrachloroethane	Butanol	Octanol
OV-3	−0.378	−0.227	−0.293	−0.157	−0.461	−0.334
OV-7	−0.569	−0.427	−0.418	−0.375	−0.557	−0.435
OV-11	−0.912	−0.627	−0.562	−0.578	−0.667	−0.571
OV-17	−1.054	−0.734	−0.619	−0.685	−0.740	−0.646
OV-22	−1.200	−0.904	−0.730	−0.793	−0.763	−0.699
OV-25	−1.259	−0.931	−0.606	−0.853	−1.015	−0.726
OV-105	−0.331	−0.135	−0.531	−0.115	−0.462	−0.366
OV-225	−1.907	−1.534	−0.676	−1.569	−0.557	−0.716
OV-330	−1.824	−1.238	−1.051	−1.682	−1.694	−1.590
QF-1	−1.165	−0.638	−1.119	−0.236	−0.723	−0.614
CW20M	−2.444	−1.730	−1.348	−2.198	−2.160	−2.071
DEGS	−2.871	−2.436	−1.992	−2.454	−2.494	−2.570
TCEP	−3.214	−2.493	−2.314	−2.546	−2.748	−2.680
PPE-5	−1.668	−1.233	−1.055	−1.248	−1.155	−1.101
QpTS	−2.627	−1.731	−1.455	−2.636	−3.098	−3.140
QPIC	−2.609	−1.897	−1.818	−1.860	−2.099	−2.074
QMES	−2.477	−1.557	−1.394	−1.683	−3.068	−3.176
QACES	−2.548	−1.589	−1.509	−1.782	−2.926	−3.215
QTAPSO	−2.346	−1.509	−1.535	−1.582	−2.453	−2.827
DPP	−1.182	−0.786	−0.657	−0.787	−0.968	−0.443
SE-30	−0.042	−0.013	−0.121	−0.104	−0.275	−0.177

(Continued on p. 476)

TABLE VII (*continued*)

Stationary phase	1-Dodecyne	Nonanal	Dioxane	Benzodioxane	N,N-Dimethyl-aniline	Anisole
OV-3	−0.175	−0.314	−0.270	−0.209	−0.081	−0.119
OV-7	−0.230	−0.442	−0.430	−0.472	−0.275	−0.291
OV-11	−0.313	−0.587	−0.618	−0.775	−0.514	−0.508
OV-17	−0.364	−0.622	−0.729	−0.944	−0.644	−0.618
OV-22	−0.406	−0.736	−0.834	−1.132	−0.884	−0.763
OV-25	−0.542	−0.771	−0.860	−1.243	−0.915	−0.835
OV-105	−0.148	−0.315	−0.190	−0.084	0	−0.033
OV-225	−0.276	−0.675	−1.011	−2.367	−1.877	−1.636
OV-330	−0.687	−1.050	−1.138	−1.638	−1.161	−1.127
QF-1	−0.226	−1.030	−0.684	−0.386	−0.377	−0.326
CW20M	−0.955	−1.339	−1.569	−2.246	−1.584	−1.585
DEGS	−1.503	−1.976	−2.184	−2.836	−2.154	−2.054
TCEP	−1.274	−2.181	−2.497	−2.981	−2.407	−2.255
PPE-5	−0.572	−1.061	−1.254	−1.614	−1.251	−1.168
QpTS	−0.958	−1.519	−1.327	−2.168	−1.419	−1.432
QPIC	−0.890	−1.740	−1.662	−2.110	−1.814	−1.621
QMES	−0.981	−1.430	−1.182	−2.038	−1.317	−1.298
QACES	−1.018	−1.030	−1.278	−2.205	−1.484	−1.362
QTAPSO	−1.042	−1.619	−1.204	−2.077	−1.520	−1.278
DPP	−0.301	−0.498	−0.610	−0.924	−0.566	−0.129
SE-30	−0.070	−0.135	−0.067	−0.114	−0.163	0.099

	Aniline	N-Methyl-aniline	2,6-Dimethyl-aniline	2-Octyne	*cis*-Hydrindane	Dihexyl ether	Trimethyl-pyridine
OV-3	−0.277	−0.164	−0.144	−0.132	−0.087	−0.145	0.142
OV-7	−0.517	−0.398	−0.377	−0.222	−0.009	−0.177	−0.118
OV-11	−0.792	−0.668	−0.649	−0.327	−0.091	−0.243	−0.341
OV-17	−0.941	−0.817	−0.804	−0.384	−0.136	−0.285	−0.520
OV-22	−1.128	−0.993	−0.985	−0.466	−0.209	−0.344	−0.689
OV-25	−1.222	−1.149	−1.092	−0.524	−0.243	−0.405	−0.734
OV-105	−0.258	−0.121	−0.100	−0.061	−0.183	−0.125	−0.370
OV-225	−2.132	−2.185	−2.223	−0.564	−1.316	0.044	−1.417
OV-330	−2.096	−1.712	−1.686	−0.637	−0.206	−0.395	−0.033
QF-1	−0.606	−0.468	−0.467	−0.016	−0.206	−0.229	−1.049
CW20M	−2.898	−2.335	−2.344	−0.783	−0.313	−0.457	−1.571
DEGS	−3.314	−2.793	−2.962	−1.102	−0.531	−0.877	−2.456
TCEP	−3.662	−3.129	−3.297	−1.161	−0.510	−0.923	−2.154
PPE-5	−1.694	−1.535	−1.518	−0.627	−0.396	−0.410	−1.128
QpTS	−3.427	−2.906	−2.528	−0.488	−0.179	−0.415	−0.897
QPIC	−2.946	−2.537	−1.528	−0.541	−0.363	−0.480	−0.391
QMES	−3.362	−2.840	−2.576	−0.350	−0.065	−0.460	−0.925
QACES	−3.395	−2.869	−2.765	−0.289	−0.016	−0.429	−1.064
QTAPSO	−3.025	−2.567	−2.612	−0.177	−0.013	−0.889	−1.199
DPP	0.069	−0.318	−0.252	−0.237	−0.255	−0.155	−0.897
SE-30	0.012	0.125	0.154	−0.019	0.176	−0.056	−0.109

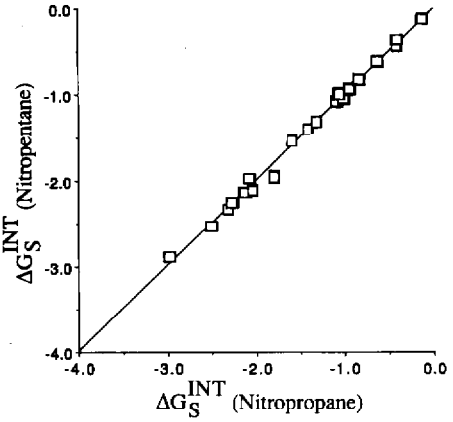

Fig. 6. Plot of ΔG_S^{INT} (nitropentane) against ΔG_S^{INT} (nitropropane) for the normal and highly cohesive stationary phases in Table I except for OV-275 and OV-225.

creases, produce a proportional change in ΔG_S^{INT} (X) for individual solutes. For an individual solute ΔG_S^{INT} (X) should depend only on the relative mole percentage of phenyl groups; for different solutes ΔG_S^{INT} (X) should depend on the strength of the intermolecular interactions with a phenyl group that exceeds those with a methyl group and the relative concentration of phenyl to methyl groups. This, again is shown to be a reasonably good approximation for different test solutes (Fig. 7). Overall, the correlation coefficients for ΔG_S^{INT} (X) against mole percentage phenyl concentration vary from $r = 0.88$ to 0.99 for the poly(methylphenyl)siloxane solvents with an average value of $r = 0.97 \pm 0.02$ ($n = 25$). ΔG_S^{INT} (X) seems to meet reasonable expectations for a solvent-dependent term to measure orientation and hydrogen bond acid–base interactions.

Prior to multivariate analysis of the data matrix of ΔG_S^{INT} (X) in Table VII, a reduction in the matrix was performed to minimize the contributions from those factors behaving anomalously or independently. The data for OV-225 and OV-275

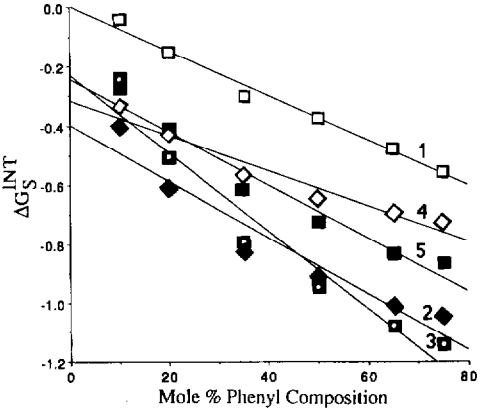

Fig. 7. Plot of ΔG_S^{INT} (X) against mole percentage phenyl for homologous series of poly(methylphenyl) siloxane solvents. 1 = *n*-butylbenzene; 2 = nitropentane; 3 = nitrobenzene; 4 = octanol; 5 = dioxane.

were removed. The low solubility of *n*-alkanes in OV-275 prevented the gas–liquid partition coefficients from being determined with similar accuracy to the other phases, as discussed previously. With OV-225 an unusual dependence on the value of ΔG_S^{INT} (X) with the absolute magnitude of the Van der Waals volume was observed. Some representative values of ΔG_S^{INT} (X) using the different Van der Waals volumes and total surface area are summarized in Table VIII. ΔG_S^{INT} (X) calculated using the

TABLE VIII

COMPARISON OF VALUES FOR ΔG_S^{INT} (X) ON SEVERAL STATIONARY PHASES CALCULATED FROM DIFFERENT VAN DER WAALS VOLUMES AND TOTAL SURFACE AREA (kcal/mol)

Test solute	Stationary phase	Van der Waals volume or surface area			
		V_A	V_I	V_X	*TSA*
Butylbenzene	OV-3	−0.045	−0.050	−0.064	0.013
	OV-17	−0.381	−0.395	−0.417	−0.302
	OV-25	−0.558	−0.555	−0.561	−0.441
	OV-225	−1.151	−1.094	−0.759	−0.622
	CW20M	−0.960	−0.959	−0.982	−0.823
	DEGS	−1.409	−1.438	−1.437	−1.213
	QMES	−0.731	−0.757	−0.760	−0.562
	QTAPSO	−0.791	−0.826	−0.839	−0.505
Nitrobenzene	OV-3	−0.252	−0.265	−0.265	−0.179
	OV-17	−0.947	−0.963	−0.963	−0.813
	OV-25	−1.141	−1.147	−1.147	−0.965
	OV-225	−2.486	−2.374	−2.374	−0.161
	CW20M	−2.294	−2.306	−2.306	−2.091
	DEGS	−2.746	−2.795	−2.795	−2.456
	QMES	−2.372	−2.375	−2.375	−2.090
	QTAPSO	−2.159	−2.232	−2.237	−1.761
Octanol	OV-3	−0.334	−0.322	−0.336	−0.315
	OV-17	−0.646	−0.645	−0.668	−0.618
	OV-25	−0.726	−0.699	−0.705	−0.675
	OV-225	−0.716	−0.800	−1.479	−1.444
	CW20M	−2.071	−2.038	−2.062	−2.020
	DEGS	−2.570	−2.536	−2.536	−2.530
	QMES	−3.176	−3.156	−3.159	−3.125
	QTAPSO	−2.827	−2.767	−2.780	−2.767
Dioxane	OV-3	−0.270	−0.243	−0.252	−0.219
	OV-17	−0.729	−0.704	−0.715	−0.608
	OV-25	−0.860	−0.809	−0.806	−0.707
	OV-225	−1.011	−1.235	−1.240	−1.137
	CW20M	−1.569	−1.504	−1.510	−1.399
	DEGS	−2.184	−2.080	−2.074	−1.964
	QMES	−1.182	−1.107	−1.102	−0.987
	QTAPSO	−1.204	−1.049	−1.050	−0.919
N,N-Dimethylaniline	OV-3	−0.081	−0.084	−0.096	−0.010
	OV-17	−0.644	−0.653	−0.672	−0.762
	OV-25	−0.915	−0.906	−0.909	−0.761
	OV-225	−1.877	−1.849	−1.259	−1.092
	CW20M	−1.584	−1.577	−1.594	−1.404
	DEGS	−2.154	−2.168	−2.166	−1.891
	QMES	−1.317	−1.330	−1.331	−1.094
	QTAPSO	−1.520	−1.536	−1.545	−1.144

total Van der Waals surface area is always less than when calculated using the computer-calculated Van der Waals volume, V_A, but is highly correlated with it. The trends predicted remain the same. For phases other than OV-225, ΔG_S^{INT} (X) calculated using V_A, V_I and V_X show acceptable agreement. OV-225 shows large variations for many solutes when different measures of the Van der Waals volume are used. There seems to be no obvious reason why ΔG_S^{INT} (X) values on OV-225 would be uniquely sensitive to the absolute value of the Van der Waals volume, given the general good correlation among the volume terms, and the fact that similar behavior was not apparent for any of the other phases listed in Table I. The experimental data for OV-225 are reproducible and this aberation is due to a real physical phenomenon on which we reserve judgement. Removing OV-225 from the data set, however, provides a better classification of solute and phase properties by removing the heavy weighting given to the characteristics of this phase by multivariate analysis.

A correlation matrix of the scaled data for ΔG_S^{INT} (X) (each variable was mean centered with a standard deviation of one) was produced to evaluate the relationship between individual variables. A correlation of 0.90 or greater was considered to be a reasonable indication that the variables are correlated, that is, displaying the same retention mechanisms. The variables meeting this test are summarized in Table IX for the two cases where it seems reasonable to assign a particular interaction as a dominant interaction as well as those test solutes that can be classified as behaving independently (uncorrelated with any other test solute with $r > 0.92$). The largest group of highly correlated test solutes have large dipole moments or are easily polarizable and it seems reasonable to associate these test solutes with strong orientation interactions. Dioxane might seem to be anomalous within this group given its small bulk dipole moment, but in fact it has been demonstrated that the local dipole moment preceived by a solvent molecule for dioxane is much greater than that predicted by the bulk dipole moment [28]. The correlation with the alkanols should not be taken as anomalous because of their strong hydrogen-bond donor properties, as they also have substantial dipole moments.

The second group of correlated test solutes is headed by the alkanols and apart from benzonitrile, nitrobenzene and nitropentane, contains solutes with proton donor properties. *n*-Octanol seems to be a reasonable test solute for probing hydrogen-bonding interactions and all the alkanols are highly correlated in the data set. All of the proton-donor solutes have significant dipole moments in addition explaining the modest correlation with benzonitrile, nitrobenzene and nitropentane. The absence of a strong proton acceptor interaction for pyridine, dioxane and benzodioxane has been discussed elsewhere [3,17]. These solutes are either retained predominantly by orientation interactions or the set of stationary phases used for the analysis does not contain a sufficient number of strong hydrogen-bond donor solvents to differentiate this mechanism. The former seems to be the most likely answer [2,3,8,16].

The remaining four solutes in Table IX show few strong correlations with other solutes (dihexyl ether, $r = 0.91$ with 1-dodecyne and nonanal and 0.90 with N,N-dimethylaniline; *cis*-hydrindane, $r = 0.92$ with 2-octyne) and must be considered as behaving independently. Three of them, *cis*-hydrindane, dihexyl ether and 2-octyne, have little orientation or proton donor–acceptor capacity and cannot be considered as selective polar solutes. Their principal interactions must be dispersive interactions and most likely the ΔG_S^{INT} (X) term consists of weak polar interactions and dispersive

TABLE IX

SUMMARY OF CORRELATED VALUES ABSTRACTED FROM THE CORRELATION MATRIX

Solute	Correlation Coefficient	Solute	Correlation Coefficient
(a) Orientation interactions		*(b) Proton donor–acceptor interactions*	
Nitrobenzene	1.00	Octanol	1.00
Benzonitrile	1.00	Butanol	0.99
Nitropentane	0.99	2-Methyl-2-pentanol	0.99
Nitropropane	0.99	Aniline	0.97
Benzodioxane	0.98	N-Methylaniline	0.97
Pyridine	0.98	2,6-Dimethylaniline	0.95
N,N-Dimethylaniline	0.97	Benzonitrile	0.92
N-Methylaniline	0.97	1-Dodecyne	0.91
1,1,2,2-Tetrachloroethane	0.97	Nitrobenzene	0.91
Anisole	0.96	Nitropentane	0.91
1-Dodecyne	0.96	*(c) Solutes behaving independently*	
Aniline	0.96	*cis*-Hydrindane	
Butylbenzene	0.95	Dihexyl ether	
2-Octanone	0.95	2-Octyne	
2,6-Dimethylaniline	0.95	2,4,6-Trimethylpyridine	
Nonanal	0.95		
Dioxane	0.94		
2-Methyl-2-pentanol	0.94		
Butanol	0.94		
Octanol	0.91		
Benzene	0.91		

interactions inadequately accounted for in eqn. 8. 2,4,6-Trimethylpyridine seems to be a genuine outsider and exhibits properties that are not even similar to pyridine [3,17].

To define better the behavior of the test solutes, the scaled data were subjected to principal component analysis. Eigenvectors were extracted from the data such that the maximum information in the form of variance was preserved with a minimum number of eigenvectors. A summary of the results is presented in Table X. Two vectors are sufficient to account for most of the variance. Eliminating the four test solutes behaving independently from the data matrix increases the cumulative variance for the first two principal components from 93.46% to 96.17%. Eliminating OV-225 from the reduced solute data set further increases the cumulative variance to 97.43% for the first two principal components. For each case the variance for the second eigenvector is reduced compared with the first and inspection of the classifications obtained indicated a more logical grouping when the independent test solutes and OV-225 and OV-275 were deleted from the data set. This left a data set containing 21 solutes separated on 20 stationary phases that was used for subsequent pattern recognition analysis.

Scrutinizing the loadings (how much each test solute contributes to the principal component) (Table XI) indicates that the first component was heavily weighted towards solutes recognizable as having a significant capacity for orientation interactions. Loading 2 is heavily weighted towards solutes recognizable as having signif-

TABLE X

SUMMARY OF EIGENVECTOR AND PRINCIPAL COMPONENT ANALYSIS OF THE DATA MATRIX

Eigenvector	Eigenvalue	Percentage variance	Percent cumulative variance
(a) All solutes in Table VII			
1	21.2426	84.97	84.97
2	2.1240	8.49	93.46
3	0.7616	3.04	96.51
4	0.3467	1.38	97.89
(b) Eliminating solutes behaving independently in Table VIII			
1	19.0773	90.84	90.84
2	1.1196	5.33	96.17
3	0.4297	2.04	98.22
(c) Eliminating OV-225 from phases in Table I with same solutes as in (b)			
1	19.6555	93.59	93.59
2	0.8054	3.83	97.43
3	0.2326	1.10	98.53

icant proton donor–acceptor capacity, the proton donor solutes having positive coefficients and the proton acceptor solutes having negative coefficients. The proton donor solutes represented by the alkanols would be expected to have a greater capac-

TABLE XI

SUMMARY OF THE LOADINGS FOR THE FIRST THREE PRINCIPAL COMPONENTS (21 SOLUTES ON 20 PHASES)

Variable	Loading 1	Variable	Loading 2	Variable	Loading 3
Benzonitrile	0.0224	Octanol	0.0439	2-Octanone	−0.0530
Nitrobenzene	0.0224	Benzene	−0.0398	Nonanal	−0.0435
Pyridine	0.0223	Butanol	0.0378	Nitropentane	−0.0300
Benzodioxane	0.0223	2-Methyl-2-pentanol	0.0345	1,1,2,2-Tetrachloroethane	0.0282
Nitropentane	0.0223	Dioxane	−0.0309	Nitropropane	−0.0259
Nitropropane	0.0222	Butylbenzene	−0.0277	Benzodioxane	0.0242
N,N-Dimethylaniline	0.0221	Aniline	0.0213	2,6-Dimethylaniline	0.0223
N-Methylaniline	0.0221	N,N-Dimethylaniline	−0.0188	Benzene	0.0207
Anisole	0.0221	N-Methylaniline	0.0186	Butylbenzene	0.0166
1-Dodecyne	0.0221	2,6-Dimethylaniline	0.0158	Anisole	0.0165
1,1,2,2-Tetrachloroethane	0.0219	Anisole	−0.0158	1-Dodecyne	0.0159
Aniline	0.0219	Pyridine	−0.0148	Aniline	0.0120
2,6-Dimethylaniline	0.0218	Nonanal	−0.0125	N-Methylaniline	0.0118
Butylbenzene	0.0217	2-Octanone	−0.0073	2-Methyl-2-pentanol	−0.0110
2-Octanone	0.0216	Benzodioxane	−0.0063	Benzonitrile	−0.0093
Nonanal	0.0216	Nitropropane	−0.0036	N,N-Dimethylaniline	0.0082
Dioxane	0.0216	1-Dodecyne	0.0032	Dioxane	−0.0048
2-Methyl-2-pentanol	0.0213	Benzonitrile	0.0028	Butanol	0.0042
Butanol	0.0212	Nitrobenzene	0.0010	Nitrobenzene	−0.0040
Octanol	0.0207	Nitropentane	0.0006	Octanol	0.0015
Benzene	0.0207	1,1,2,2-Tetrachloroethane	0.0001	Pyridine	−0.0001

ity for solvent proton acceptor interactions than the proton acceptor solutes typified by benzene, dioxane, butylbenzene and N,N-dimethylaniline as the four most heavily weighted solutes for solvent proton donor interactions. These solutes would normally be considered weak hydrogen-bond bases and most likely better test solutes could be found to represent this interaction. The weak weighting of loading 2 towards orientation solutes indicates reasonable discrimination of properties. Loading 3 seems to be most heavily weighted towards solutes with a combination of moderate dipole and moderate proton donor–acceptor properties and provides a less clearly defined axis for discrimination. However, loading 3 is headed by solutes only moderately weighted in loading 2, so it should provide a complementary classification of stationary phase properties.

The plot of loading 1 (orientation) against loading 2 (proton donor–acceptor) and loading 1 against loading 3 (Fig. 8) provides a classification of the solutes as to type. In the plot of loading 1 against 2 solutes exhibiting essentially orientation interactions are distributed along the central axis. Those solutes with the largest dipole moments are located towards the right-hand side of the figure. The alcohols are closely grouped in the upper left hand portion of the plot and are suitable test solutes for solvent proton acceptor interactions. A secondary group displaced from the central axis consisting of aniline, N-methylaniline and 2,6-dimethylaniline also shows significant proton donor capacity. The test solutes for solvent proton donor capacity are diffusely scattered in the lower proton of the plot and are not as effective as the alkanols at defining a particular interaction. The loading plot 1 against 3 shows little clustering confirming the non-discriminate nature of axis 3 for identifying solutes with significant proton donor–acceptor interactions.

In the same manner that the principal component plots of the loadings can be used to classify the test solutes, the scores plots can be used to classify the stationary phases based on their interactions with the test solutes (Fig. 9). Score 1 against score 2 forms a tight cluster with the liquid organic sulfonate salts (QpTS, QTAPSO, QACES, and QMES) exhibiting strong orientation and proton acceptor properties, uniquely different to the other phases. Slightly more diffuse is the group (TCEP, DEGS, CW 20M, and QPIC, which exhibit strong orientation interactions. The third group contains the poly(siloxanes) SE-30, OV-105, OV-3, OV-7, OV-11, OV-17, OV-22 and OV-25, showing increasing polarity as the mole percentage of phenyl groups is increased. PPE-5 and QF-1 are on the boundary of this group while OV-330 is close to the center of the crosshairs, indicating a balance between orientation and proton donor–acceptor interactions. Score 1 against 3 shows less clustering although groups 1 and 3, discussed above, can still be discerned, if less distinctly than the plot of score 1 against score 2. QF-1 is now seen to behave independently. QF-1 is known to show selectivity for ketone groups. Loading 3 is heavily weighted towards 2-octanone, explaining this change in position. Overall, the score plots provide a logical and intuitive classification of the phases supporting the general usefulness of the solvent model presented in this paper. In general, the method chosen to estimate the molecular volume of solutes and *n*-alkanes is not too important when a reference hydrocarbon solvent is used to compensate for deficiencies in the assumption that the hard sphere volume of the molecules is proportional to the contact surface of the cavity. The strength of the ΔG_S^{INT} (X) parameter is the very high degree of correlation observed for the behavior of solutes of a similar kind in a wide range of solvents and its

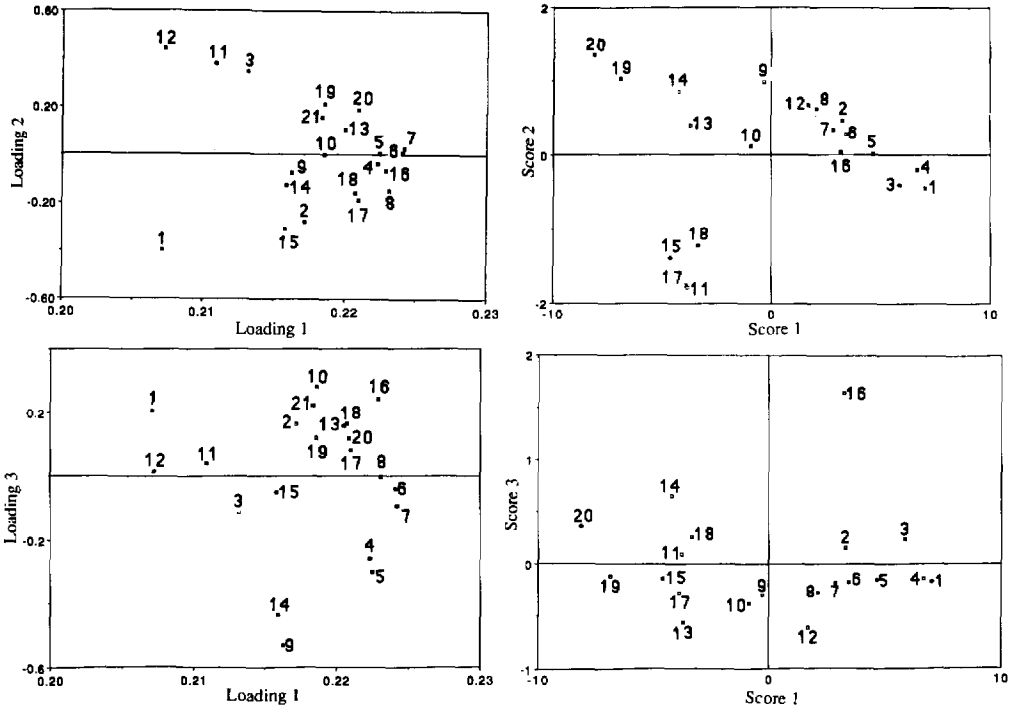

Fig. 8. Principal component plots of loading 2 and loading 3 against loading 1. Test solutes are identified in Table I (number on axis × 10).

Fig. 9. Principal component plots of score 2 and score 3 against score 1. Stationary phases are identified in Table I.

ability to classify solvents in accordance to their capacity for orientation and proton donor–acceptor interactions in a logical manner.

In conclusion, the parameter ΔG_S^{INT} (X) has been shown to provide a quantitative measure of solute–solvent orientation and proton donor–acceptor interactions that are independent of solute size. ΔG_S^{INT} (X) can be simply determined from experimental values for the partial molal Gibbs free energy of solution of solute (X) and appropriate *n*-alkanes on solvent S and squalane and can be determined for any phase in which the solute (X) and *n*-alkanes are sufficiently soluble to provide reasonable values for the gas–liquid partition coefficient.

REFERENCES

1 C. F. Poole and S. A. Schuette, *Contemporary Practice of Chromatography*, Elsevier, Amsterdam, 1984, p. 42.
2 C. F. Poole and S. K. Poole, *Chem. Rev.*, 89 (1989) 377.
3 S. K. Poole and C. F. Poole, *J. Chromatogr.*, 500 (1990) 329.
4 R. V. Golovnya and T. A. Misharina, *J. High Resolut. Chromatogr. Chromatogr. Commun.*, 3 (1980) 4.
5 J. A. Yancey, *J. Chromatogr. Sci.*, 24 (1986) 117.
6 M. V. Budahegyi, E. R. Lombosi, T. S. Lombosi, S. Y. Meszaros, Sz. Nyiredy, G. Tarjan, I. Timar and J. M. Takacs, *J. Chromatogr.*, 271 (1983) 213.

7 B. R. Kersten, C. F. Poole and K. G. Furton, *J. Chromatogr.*, 411 (1987) 43.
8 B. R. Kersten, S. K. Poole and C. F. Poole, *J. Chromatogr.*, 468 (1989) 235.
9 S. K. Poole, B. R. Kersten and C. F. Poole, *J. Chromatogr.*, 471 (1989) 91.
10 C. F. Poole, S. K. Poole, R. M. Pomaville and B. R. Kersten, *J. High Resolut. Chromatogr. Chromatogr. Commun.*, 10 (1987) 670.
11 C. E. Figgins, T. H. Risby and P. C. Jurs. *J. Chromatogr. Sci.*, 14 (1976) 453.
12 R. V. Golovnya and T. A. Misharina, *J. High Resolut. Chromatogr., Chromatogr. Commun.*, 3 (1980) 51.
13 K. G. Furton and C. F. Poole, *J. Chromatogr.*, 399 (1987) 47.
14 J. Novak, *J. Chromatogr.*, 78 (1973) 269.
15 M. Roth and J. Novak, *J. Chromatogr.*, 234 (1982) 337.
16 B. R. Kersten and C. F. Poole, *J. Chromatogr.*, 452 (1988) 191.
17 T. O. Kollie and C. F. Poole, *J. Chromatogr.*, 550 (1991) 213.
18 M. H. Abraham, R. M. Doherty, M. J. Kamlet and R. W. Taft, *Chem. Br., 22 (1986) 551.*
19 M. J. Kamlet, R. M. Doherty, J.-L. M. Abboud, M. H. Abraham and R. W. Taft, *Chemtech*, (1986) 566.
20 R. W. Taft, J.-L. M. Abboud, M. J. Kamlet and M. H. Abraham, *J. Solution Chem.*, 14 (1985) 153.
21 M. H. Abraham, P. L. Grellier, R. A. McGill, R. M. Doherty, M. J. Kamlet, T. N. Hall, R. W. Taft, P. W. Carr and W. J. Koros, *Polymer*, 28 (1987) 1363.
22 M. H. Abraham and R. Fuchs, *J. Chem. Soc., Perkin Trans. 2*, (1988) 523.
23 M. H. Abraham, P. L. Greillier, I. Hamerton, R. A. McGill, D. V. Prior and G. S. Whiting, *Faraday Discuss. Chem. Soc.*, 85 (1988) 107.
24 M. H. Abraham, G. S. Whiting, R. M. Doherty and W. J. Shuley, *J. Chromatogr.*, 518 (1990) 329.
25 L. R. Snyder, *J. Chromatogr.*, 92 (1974) 223.
26 L. R. Snyder, *J. Chromatogr. Sci.*, 16 (1978) 223.
27 H. Poppe and E. H. Slaats, *Chromatographia*, 14 (1981) 89.
28 M. J. Kamlet, R. W. Taft, P. W. Carr and M. H. Abraham, *J. Chem. Soc., Faraday Trans. 1*, 78 (1982) 1689.
29 S. C. Rutan, P. W. Carr and R. W. Taft, *J. Phys. Chem.*, 93 (1989) 4292.
30 S. C. Rutan, P. W. Carr, W. J. Cheong, J. H. Park and L. R. Snyder, *J. Chromatogr.*, 463 (1989) 21.
31 W. J. Cheong and P. W. Carr, *J. Chromatogr.*, 500 (1990) 215.
32 M. H. Abraham, A. Nasehzadeh, J. J. Moura Ramos and J. Reisse, *J. Chem. Soc., Perkin Trans. 2*, (1980) 854.
33 C. F. Poole, R. M. Pomaville and T. A. Dean, *Anal. Chim. Acta*, 225 (1989) 193.
34 R. M. Pomaville and C. F. Poole, *Anal. Chem.*, 60 (1988) 1103.
35 A. Bondi, *J. Phys. Chem.*, 68 (1964) 441.
36 J. C. McGowan, *J. Appl. Chem. Biotechnol.*, 28 (1978) 599.
37 J. C. McGowan, *J. Chem. Tech. Biotechnol.*, 34A (1984) 38.
38 M. H. Abraham and J. C. McGowan, *Chromatographia*, 23 (1987) 243.
39 D. E. Leahy, *J. Pharm. Sci.*, 75 (1986) 629.
40 D. E. Leahy, P.W. Carr, R. S. Pearlman, R. W. Taft and M. J. Kamlet, *Chromatographia*, 21 (1976) 473.
41 M. J. Kamlet, R. M. Doherty, P. W. Carr, D. Mackay, M. H. Abraham and R. W. Taft, *Environ. Sci. Technol.*, 22 (1988) 503.
42 F. Mohamadi, N. G. J. Richards, W. C. Guida, R. Liskamp, M. Lipton, C. Caufield, G. Chang, T. Hendrickson and W. C. Still, *J. Comput. Chem.*, 11 (1990) 440.
43 J. B. Moon and W. J. Howe, *J. Mol. Graphics*, 7 (1989) 109.
44 R. S. Bohacek and W. C. Guida, *J. Mol. Graphics*, 7 (1989) 113.
45 R. S. Pearlman, in S. H. Valkowsky, A. A. Sinkula and S. C. Valvani (Editor), *Physical and Chemical Properties of Drugs*, Marcel Dekker, New York, 1980, p. 321.
46 W. J. Dunn, J. H. Block, and R. S. Pearlman, *Partition Coefficients. Determination and Estimation*, Pergamon Press, New York, 1986.
47 P. Camilleri, S. A. Watts and J. A. Boraston, *J. Chem. Soc., Perkin Trans. 2*, (1988) 1699.
48 B. K. Lee and F. M. Richards, *J. Mol. Biol.*, 55 (1971) 379.